Soft Matter

PAPER

View Article Online
View Journal

Attachment/detachment hysteresis of fiber-based magnetic grabbers†

Cite this: DOI: 10.1039/c3sm53025f

Yu Gu and Konstantin G. Kornev*

We developed an experimental protocol to analyze the behaviour of a model fiber-based magnetic grabber. A fiber is vertically suspended and fixed to the substrate by its upper end. A magnetic droplet is attached to the free end of the fiber and when a permanent magnet approaches the droplet, the fiber is forced to bow and finally jumps to the magnet. It appears that one can flex the micro-fibers by very small micro or even nano-Newton forces. Using this setup, we discovered a hysteresis of fiber attachment/detachment: the pathway of the fiber jumping to and off the magnet depends on the distance between the magnet and the clamped end. This phenomenon was successfully explained by the Euler–Benoulli model of an elastic beam. The observed hysteresis of fiber attachment/detachment was attributed to the multiple equilibrium configurations of the fiber tip placed in a dipole-type magnetic field.

Received 3rd December 2013
Accepted 15th January 2014

DOI: 10.1039/c3sm53025f

www.rsc.org/softmatter

Introduction

Flexibility is the most attractive feature of fibers allowing them to be twisted into yarns and weaved into fabrics.[1] Fibers can be made solid, porous or hollow and can be produced in different cross-sectional shapes. Thus, fibers constitute a broad class of flexible, lightweight structures that can be utilized in many applications.[2] Progress in the micro and nanofiber formation and in the development of new applications of fibers such as sensors, manipulators, and artificial muscles, calls for a new level of understanding of the mechanisms of fiber actuation with external fields when the force is limited to the micro-and nano-Newton scale.[3–9] Fiber manipulation and measurement of such small forces require special tools and transducers.[3,4] In the earlier paper,[5] we proposed to use nanofiber yarns to grab microdroplets of hazardous fluids. It has been shown that the fiber-based grabber can be remotely controlled by applying a nonuniform external magnetic field[5,6] thus eliminating the need for a special transducer. In this paper, we study a fiber-based grabber with a magnetic tip and demonstrate an interesting physical phenomenon specific for this type of grabbers: the pathway of tip attachment appeared distinct from the pathway of tip detachment.

Four decades ago, Moon with colleagues published several papers on bending of thin magnetic plates by applying a uniform magnetic field.[10,11] The effect of a nonuniform magnetic field on the bending of a continuous magnetic fiber has been discussed in ref. 6. It was found that a continuous magnetic fiber is attracted to the electromagnet at a current which appeared different from the current at which the fiber springs back from the electromagnet. Since the magnetic moment of each element of a continuous fiber tends to align along the external field, the fiber is subject to a non-uniform magnetic torque. Therefore, attraction/retraction hysteresis in a non-uniform field was attributed to the non-uniform mechanical torque exerted on the magnetic material.

In this paper we eliminate the effect of nonuniform magnetic torque by making only the fiber tip magnetic. The torque on the tip is proven to be negligible and the fiber bends because of the field gradient. Using the experimental setup shown in Fig. 1, the specifics of the fiber bending with the magnetic field are revealed. Moon and Holmes[12] were probably the first who paid attention to the unusual properties of a macroscopic beam with a magnetic tip. They studied the vibration behavior of a beam in a nonuniform field of a special configuration and discovered a strange attractor in the dynamic system describing the beam

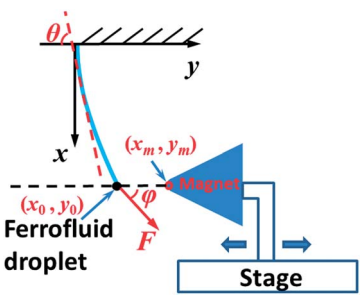

Fig. 1 Schematic of the experimental setup. The fiber profile is described by angle θ (x, y) formed by the tangent line to the fiber at point (x, y) with the y-axis, φ is the angle between the magnetic force **F** and the y-axis.

Department of Materials Science and Engineering, Clemson University, Clemson, SC, 29634, USA. E-mail: kkornev@clemson.edu; Tel: +1 8646566541

† Electronic supplementary information (ESI) available. See DOI: 10.1039/c3sm53025f

oscillations. Free suspended filaments with magnetic ends recently attracted attention as possible candidates for the development of artificial microswimmers.[9] The attachment/detachment hysteresis has not been mentioned in these studies.

In a model magnetic grabber shown in Fig. 1, one end of a fiber is fixed at point (0, 0) and the end (x_0, y_0) is free to move. A droplet of magnetic glue is attached to the free end of the fiber. The fiber bending is caused by the magnetic force acting on the magnetic glue,

$$\mathbf{F} = (\mathbf{m}\cdot\nabla)\mathbf{B} \quad (1)$$

where **m** is the magnetic moment of the droplet and **B** is the external magnetic field. When a magnet pulls the droplet, the fiber bends toward the magnet and when the magnet is removed, the fiber springs back. A glass fiber with purely elastic behavior was chosen to demonstrate an interesting behaviour of this magnetic grabber making a distinct pathway when it sways toward and jumps off from the magnet. This hysteresis is analyzed using the Euler–Benoulli model of an elastic beam and is confirmed by the experiments.

Most recently, the buckling instability induced by a magnetic torque has been studied for a macroscopic beam[13] when a permanent magnet was attached to the end of the beam and a uniform magnetic field was used to apply the torque. No hysteresis was observed.[13] The mechanism of buckling instability reported in the present paper is therefore different from that observed in ref. 13. This difference places the observed attachment/detachment hysteresis into a new category of physical phenomena specific for a non-uniform field.

It is believed that the attachment/detachment hysteresis can be used to design fiber-based grabbers enabling one to bring the desired object to the pole of a magnet and then move it further to an analytical device keeping the fiber end attached to the magnet. This operation is required, for example, in microfluidic analytical devices dealing with droplets of hazardous liquids.[5]

The distinct pathways of fiber attachment to and detachment from the magnet

Setup and materials

Magnetic glue with superparamagnetic nanoparticles is attached to the fiber tip (see Materials & methods for the details). The magnetic moment of a glue droplet is proportional to the droplet size.[14] Magnetic moments of superparamagnetic nanoparticles exactly follow the applied magnetic field without exerting any torque on the fiber tip. Hence from eqn (1), the force magnitude and its direction can be controlled by the field gradient and the size of the magnetic droplet. This method of force application allows one to generate extremely small forces not interfering with the mechanical response of the fiber itself.

A cone shaped magnet (SuperMagnetMan, 12.7 mm × 12.7 mm, N50 grade) is attached to a linear stage (VT-21, MICOS). The *y*-axis is aligned with the magnet axis as shown in Fig. 2(a). The linear stage with the magnet moves parallel to the *y*-axis so that

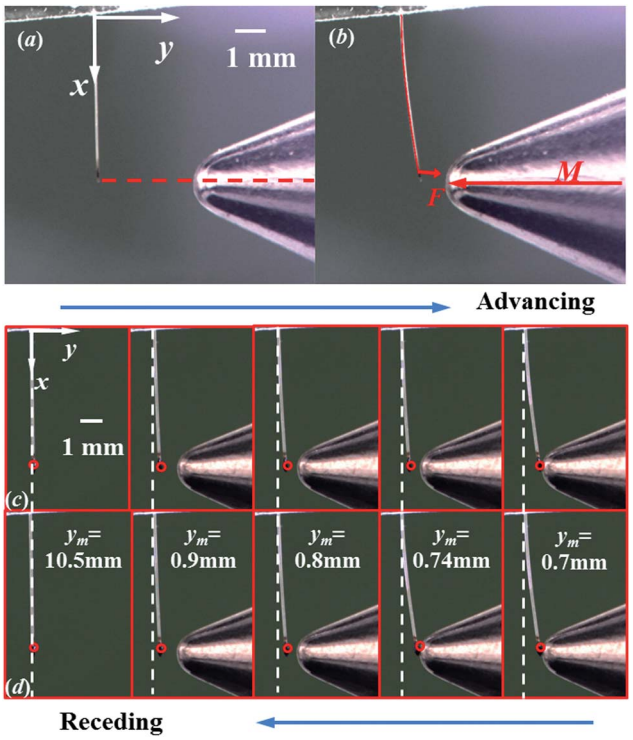

Fig. 2 (a) Magnet approaching the fiber (b) fiber bends toward the magnet pole when the magnet comes in close proximity to the fiber end with the magnetic droplet. The red curve corresponds to the theoretical description of the fiber profile calculated from eqn (10) with $E = 2.8$ GPa, $I = 2.83 \times 10^{-19}$ m^4, F = 9.6 μN, $\varphi = 0.01$ rad, and $D =$ 50 μm. (c) Attachment and (d) detachment pathways of deformation of a 100 μm diameter glass fiber.

the fiber bends only in the *xy* plane. When the magnet is far away from the fiber tip, no bending is observed. When the magnet approaches the fiber, the droplet tends to come to the pole of the magnet forcing the fiber to flex toward the pole, Fig. 2(b).

The reference point (0, 0) is chosen as the point where the fiber is clamped to the substrate. We always associate the fiber attachment with the movement of magnet toward the clamped end. Accordingly, the fiber detachment is associated with the movement of the magnet away from the clamped end. The magnet position is quantified by the pair (x_m, y_m) as shown in Fig. 1. In this reference frame, the movement of the fiber tip can be clearly observed and traced by following the change of parameters (x_m, y_m). In all experiments, the magnet was moving parallel to the *y*-axis, hence parameter x_m was fixed choosing this special reference frame, and by doing this one can independently specify the positions of the fiber tip and the magnet. This procedure allows one to avoid confusion with the simultaneous movement of the fiber and the magnet.

Force balance of the deformed fiber in a magnetic field

Observations on the fiber behavior in Fig. 2(c) and (d) when the magnet approaches position $y_m = 0.74$ mm, and then recedes back, suggest that the elastic glass fiber with a magnetic droplet distinguishes advancing strike from the receding one. When the

magnet moves toward the fiber, the fiber tip stays separated from the magnet. Contrary to that, when the tip has already been attached to the magnet and the magnet moves back, the tip does not want to leave the magnet.

The competition between two forces, elastic $\mathbf{F}_e$ and magnetic $\mathbf{F}_m$, governs the fiber flexing. The magnetic force was calculated using the field distribution shown in Fig. 3. Substituting the field gradient taken from Fig. 3(a) into eqn (1), we calculated magnetic force $\mathbf{F}_m$. The magnetic moment of the drop was measured by using the Alternating Gradient Magnetometer (AGM 2900, Princeton Measurements Inc., NJ, USA).

In all experiments, the x component of magnetic force is much smaller than the y-component, hence angle φ in Fig. 1 is approximately zero, $\mathbf{F}_m = (0, F_m)$ (see Fig. 3(b) and ESI S1 for the details†). Thus, the magnetic force is considered acting only in the y-direction.

When the fiber reaches its equilibrium state, magnetic and elastic forces are balanced $\mathbf{F}_e + \mathbf{F}_m = 0$. In order to make the physical picture clear, we first consider small deflections of the fiber tip. Assuming for a moment that the fiber tip is displaced by a mechanical force $\mathbf{F}_{mech} = (0, F_{mech})$. From the theory of elastic beams, the fiber profile is described by the following equation[15]

$$EI\frac{d^3y}{dx^3} + F_{mech} = 0, \quad (2)$$

where E is the Young's modulus and I is the second moment of inertia of the fiber cross-section. For a cylindrical fiber of diameter d, the second moment of inertia is related to the diameter as $I = \pi d^4/64$.[15] Eqn (2) is subject to the following boundary conditions:

$$\begin{cases} y = 0 & \text{at } x = 0, \\ dy/dx = 0 & \text{at } x = 0, \\ d^2y/dx^2 = 0 & \text{at } x = L. \end{cases} \quad (3)$$

By solving this linear problem of elasticity, the profile of the deformed fiber is obtained as

$$y = \frac{F_{mech}}{6EI}x^2(3L - x). \quad (4)$$

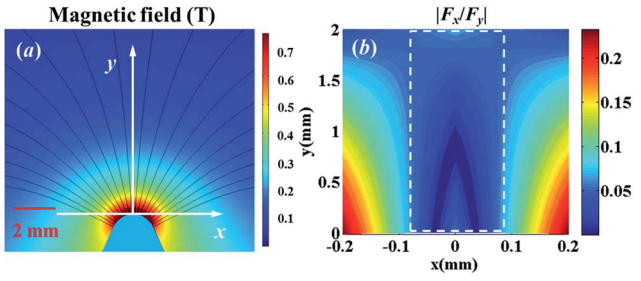

Fig. 3 (a) Magnetic field distribution in the vicinity of the magnetic pole. Color represents the magnitude of magnetic field. (b) The ratio between the x- and y-components of the magnetic force. The dashed rectangle contains the ratios of these force components corresponding to the tip location in the reported experiments: these results suggest that the x-component of magnetic force can be safely neglected as being much smaller than the y-component.

Substituting $x = L$ into eqn (4), one can determine the mechanical force F_{mech} applied to the fiber tip as a function of the tip position (x_0, y_0):

$$F_{mech} = \frac{3EI}{L^3}y_0. \quad (5)$$

In order to make the bow equivalent to that caused by the magnetic force $\mathbf{F}_m$, one needs to find the conditions when the fictitious force $\mathbf{F}_{mech}$ becomes equal to the magnetic force $\mathbf{F}_m$. Magnetic force $\mathbf{F}_m$ depends on the coordinates of the magnetic tip. Within the linear beam theory, eqn (2) and (3), the x-coordinate of the fiber tip does not change, $x_0 = L$, only the y-coordinate, y_0, changes.[15] In Fig. 1, this case corresponds to $x_0 = x_m = L$. When magnetic force $\mathbf{F}_m$ becomes equal to the fictitious force $\mathbf{F}_{mech}$, one can say that the fiber finds its equilibrium configuration because the fictitious force $\mathbf{F}_{mech}$ becomes exactly equal to the force of elastic reaction $\mathbf{F}_e$ of the fiber itself.

Hysteresis mechanism

From eqn (1) and calculated field distribution, Fig. 3, it follows that magnetic field $\mathbf{B}$ and magnetic force $\mathbf{F}_m$ are parallel to the y-axis. In order to analyze the equilibrium positions of the fiber tip, a magnetic force was calculated numerically using eqn (1) and approximated analytically. In the region $0 < y_m - y_0 < 2$ mm, the following approximation was set up

$$F_m = \frac{F_0}{[\beta_m(y_m - y_0) + 1]^\alpha} \quad (6)$$

where F_0 is the magnetic force acting on the magnetic droplet when the tip is attached to the magnet, $y_0 = y_m$. This force is proportional to the droplet volume. The constant β_m (measured in m^{-1}) is related to the curvature of the magnet and it does not depend on the droplet volume. The proposed approximation can describe the fields generated by different magnets. For the experiments shown in Fig. 2, these parameters were found by fitting the numerically calculated magnetic force with eqn (6). We found that a dipole-type field distribution with $\alpha = 3$, $F_0 = 1.04$ mN, and $\beta_m = 425$ m^{-1} approximates with the numerical solution fairly well. The detailed fitting procedure can be found in the ESI (S1).†

Fig. 4 shows the dependences of magnetic force F_m and fictitious mechanical force F_{mech} on the tip position y_0. In this figure, the tip coordinate y_0 ($y_0 \leq y_m$) is specified for four different cases depending on the position of the magnet, y_m. The crossing points between two curves correspond to the possible equilibrium when the fictitious mechanical force becomes equal to the elastic reaction of the fiber on the given magnetic force.

In Fig. 4(a) and (b), the magnet is shown far away from the fiber ($y_m = 0.9$ mm, 0.8 mm). In this case, the fiber profile does not depend on the prehistory of loading: one obtains the same profile bringing the magnet toward the fiber or moving the magnet away from the fiber. There is always a single intersection between these curves within the span of interest, $y_0 < y_m$. However, there exists another non-physical equilibrium point with $y_0 > y_m$ where the fiber tip is supposed to lie inside the magnet. This position corresponds to an unstable equilibrium that cannot be realized in

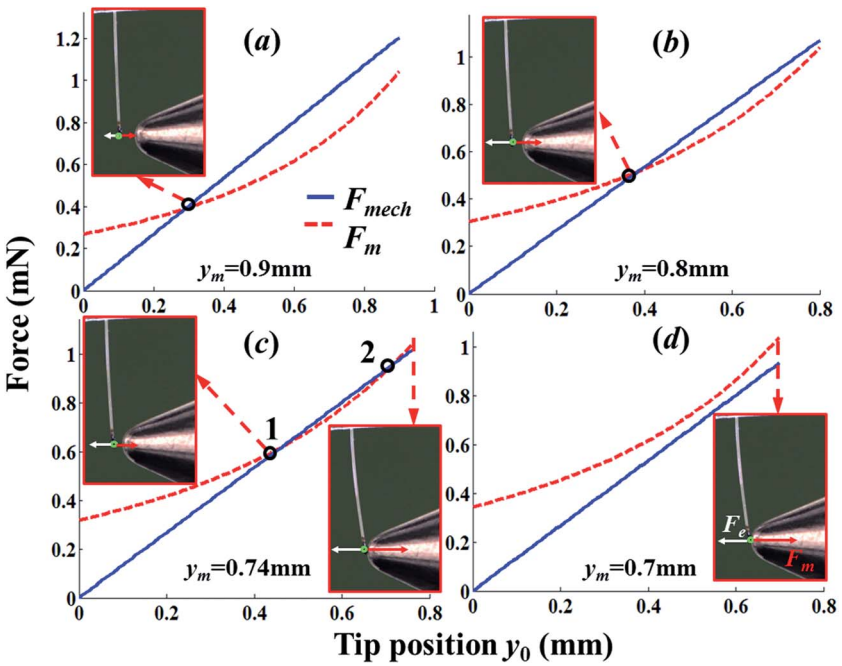

Fig. 4 Magnetic and fictitious mechanical forces as functions of position y_0 of the fiber free end. These forces depend on the position of the magnetic pole. The dashed curve corresponds to magnetic force F_m and the solid curve corresponds to fictitious mechanical force F_{mech}. The elastic modulus of fiber is $E = 17$ GPa, fiber length is $L = 5.72$ mm, and fiber diameter is $d = 100$ μm.

the experiments: any perturbation would displace the fiber tip either to the first intersection or to the magnet surface ($y_0 = y_m$). At the magnet, the fictitious mechanical force would become smaller than the magnetic one, $F_{mech}(y_m) < F_m(y_m)$. These two possibilities are illustrated in the insets of Fig. 4(c) corresponding to $y_m = 0.74$ mm.

The condition of neutral equilibrium corresponds to the moment when the conditions of tip attachment exactly match the conditions of tip detachment. The condition of tip attachment requires that both functions $F_{mech}(y_0)$ and $F_m(y_0)$ and their derivatives are equal to each other at y_0^* when the magnet is positioned at y_m^*:

$$\begin{cases} F_{mech}(y_0^*) = F_m(y_0^*) \\ \left.\dfrac{\partial F_{mech}(y_0)}{\partial y_0}\right|_{y_0=y_0^*} = \left.\dfrac{\partial F_m(y_0)}{\partial y_0}\right|_{y_0=y_0^*} \end{cases}, \text{ or } \begin{cases} \dfrac{3EI}{L^3} y_0^* = \dfrac{F_0}{\left[\beta_m(y_m^* - y_0^*) + 1\right]^{\alpha}} \\ \dfrac{3EI}{L^3} = \dfrac{\alpha\beta_m F_0}{\left[\beta_m(y_m^* - y_0^*) + 1\right]^{\alpha+1}} \end{cases}. \quad (7)$$

The existence of two possible equilibrium positions of the fiber tip leads to the different pathways of attachment of the fiber to the magnet and detachment from the magnet. When the magnet moves toward the fiber and stops at the point $y_m = 0.74$ mm, the fiber tip appears to be happily sitting at the first intersection point. However, if the fiber has already been attached to the magnet and the magnet moves away and stops at the same point $y_m = 0.74$ mm, the fiber remains attached to the magnet. In this case, the magnetic force is still stronger than the elastic force and hence the fiber tip remains stuck to the magnet.

When the magnet is even closer to the clamped end of the fiber, as shown in frame with $y_m = 0.7$ mm in Fig. 4(d), the magnetic force is always stronger than the elastic force and there are no intersection points between these curves. This implies that the fiber tip will always be attached to the magnet in this range of parameters.

Solving eqn (7) for y_0^* and y_m^*, one obtains

$$\begin{cases} y_0^* = \left[\dfrac{F_0 L^3}{3EI(\alpha\beta_m)^{\alpha}}\right]^{\frac{1}{\alpha+1}}, \\ y_m^* = y_0^* + \dfrac{1}{\beta_m}\left[\left(\dfrac{F_0 L^3 \alpha\beta_m}{3EI}\right)^{\frac{1}{\alpha+1}} - 1\right]. \end{cases} \quad (8)$$

Solutions (8) determine the position of the fiber tip y_0^* right before it jumps to the magnet. The condition for tip detachment requires that two functions $F_m(y_0)$ and $F_{mech}(y_0)$ intersect at $y_0 = y_m$. Using first eqn (7), the detachment condition is represented as:

$$y_0^* = y_m^* = \frac{F_0 L^3}{3EI}. \quad (9)$$

The neutral equilibrium condition requires that both solutions (8) and (9) are satisfied by the same pair y_0^* and y_m^*,

i.e. two intersection points in Fig. 4 merge at $y_0^* = y_m^*$ and the conditions of fiber attachment and detachment are the same. Solutions (8) and (9) are not limited to the cone magnet and specific materials of fibers used in this work. For a particular magnet, one can adjust parameters α, F_0 and β_m in eqn (6) to obtain the best fit with the numerical solution of the corresponding magnetostatic problem. In order to observe this hysteresis phenomena, one has to satisfy the following conditions $y_m^* > y_0^*$, *i.e.* $F_0 L^3 \alpha \beta_m > 3EI$ obtained from eqn (8) and ensure that the chosen magnet and beam are the appropriate pair.

The attachment/detachment hysteresis is demonstrated by the ESI video (S2).† The magnet was moved by a programmable manipulator with the step of 20 μm. After each step it was stopped for about 2 s before making the next step. After each step we observed an almost instantaneous change of the fiber profile (at the frame rate of 30 fps) from one equilibrium configuration to the other. Each type of fiber was tested five times and the resulting profiles were repeatable. At the very last step of the manipulator moving toward/away from the clamped end, *i.e.* when the fiber was about to jump to/off the magnet, we were not able to detect any difference between the dynamics of attachment and detachment of the fiber tip. In other words, the employed frame rate of the camera was not sufficient to trace the features of the tip movement. The dynamic features of the fiber attachment to/detachment from the magnet are expected to show up within the very short last step of manipulator movement. This high speed visualization of the fiber movement deserves special attention and is not considered in this paper. However, all intermediate movements of the fiber movement were reproducible and one can state that the observed phenomenon can be described within the quasi-static approximation and the effects caused by inertial forces can be neglected.

This analysis shows that the competition between elastic and magnetic forces can lead to an interesting phenomenon that distinguishes the pathways of fiber attachment to/detachment from the magnet. It appears that the effect depends mostly on the field configuration. Namely, the strength of the field gradient is important. The effect seems independent of the materials properties of the fiber: even the purely elastic fiber will show this hysteresis of attachment/detachment. In order to confirm this statement, we examined polymeric fibers with a more complex structure organization.[16]

Distinct pathways of attachment/detachment of the fiber tip at large deflections

In order to study the effect of polymer on the fiber bending characteristics, we conducted a series of experiments with Nylon 66 (DuPont), Kevlar (DuPont), and Nylon fishing line (POKKE). Fig. 5 illustrates a typical behavior of these polymeric fibers. The linear theory of elastic beams is not appropriate in this case because of the large deflections. We therefore employed the nonlinear Euler elastica equation:

$$EI\frac{d^2\theta}{dl^2} - F_{mech}\sin(\theta - \varphi) = 0. \quad (10)$$

The following boundary conditions were imposed:

$$\begin{cases} \theta = \dfrac{\pi}{2} \text{ at } l = 0, \\ \dfrac{d\theta}{dl} = 0 \text{ at } l = L. \end{cases} \quad (11)$$

The assumption that the magnetic force is directed along the y-axis is still valid: numerical analysis shows that the x-component of magnetic force $\mathbf{F}_m$ is much smaller than its y-component (Fig. 3(b)). Therefore, only the y-component of magnetic force is considered, $\mathbf{F}_m = (0, F_m)$. Hence in the definition of fictitious mechanical force we put $\varphi = 0$, $\mathbf{F}_{mech} = (0, F_{mech})$. Solution to the Euler elastica equation is given in ref. 15. Using this solution, the tip coordinates (x_0, y_0) and fiber length L are given as:

$$L = \sqrt{\frac{EI}{2F_{mech}}}\alpha(\theta_0), \quad \alpha(\theta_0) = \int_{\theta_0}^{\pi/2} \frac{d\theta}{\sqrt{\cos\theta_0 - \cos\theta}}, \quad (12)$$

$$y_0 = \sqrt{\frac{IE}{2F_{mech}}}\beta(\theta_0), \quad \beta(\theta_0) = \int_{\theta_0}^{\pi/2} \frac{\cos\theta}{\sqrt{\cos\theta_0 - \cos\theta}} d\theta, \quad (13)$$

$$x_0 = \sqrt{\frac{2EI}{F_{mech}}}\cos\theta_0, \quad (14)$$

where θ_0 corresponds to the angle $\theta_0 = \theta(x_0, y_0)$ that the fiber tip (x_0, y_0) makes with the y-axis in Fig. 1. Fig. 6 shows that both α- and β-integrals monotonously increase with $\cos\theta_0$. In all experiments, the cosine theta was bound from above by 0.5: its maximum value, $\cos\theta_0 \approx 0.4$, was observed when the magnet moved back from the clamped point reaching the position $y_m = 1.5$ mm in the receding mode. It appears that in this limited range of arguments, $\cos\theta_0 < 0.5$, two integrals are well approximated by the polynomial functions, Fig. 6.

Using these approximations, one can solve eqn (12) and (13) for F_{mech} and $\cos\theta_0$. Then the fictitious mechanical force F_{mech} and the x-coordinate of the fiber tip x_0 can be determined as functions of y_0:

$$F_{mech} \approx 3.19\frac{EI}{L^3}y_0, \quad (15)$$

$$x_0 \approx L - 0.615\frac{y_0^2}{L}. \quad (16)$$

Knowing the tip trajectory $(x_0(y_0), y_0)$ as a function of y_0, magnetic force F_m was calculated numerically along this tip trajectory. The corresponding forces F_{mech} and F_m are shown in Fig. 5(b). The crossing points corresponding to the equality $F_{mech} = F_m$ provide the balance between the magnetic force acting on the fiber tip and the elastic reaction force.

This force analysis correctly describes the observed bending hysteresis. The fiber jumped to the magnet at $y_m = 1.25$ mm when the magnet was advancing and jumped off the magnet at $y_m > 1.5$ mm when the magnet was receding. Fitting the shape of

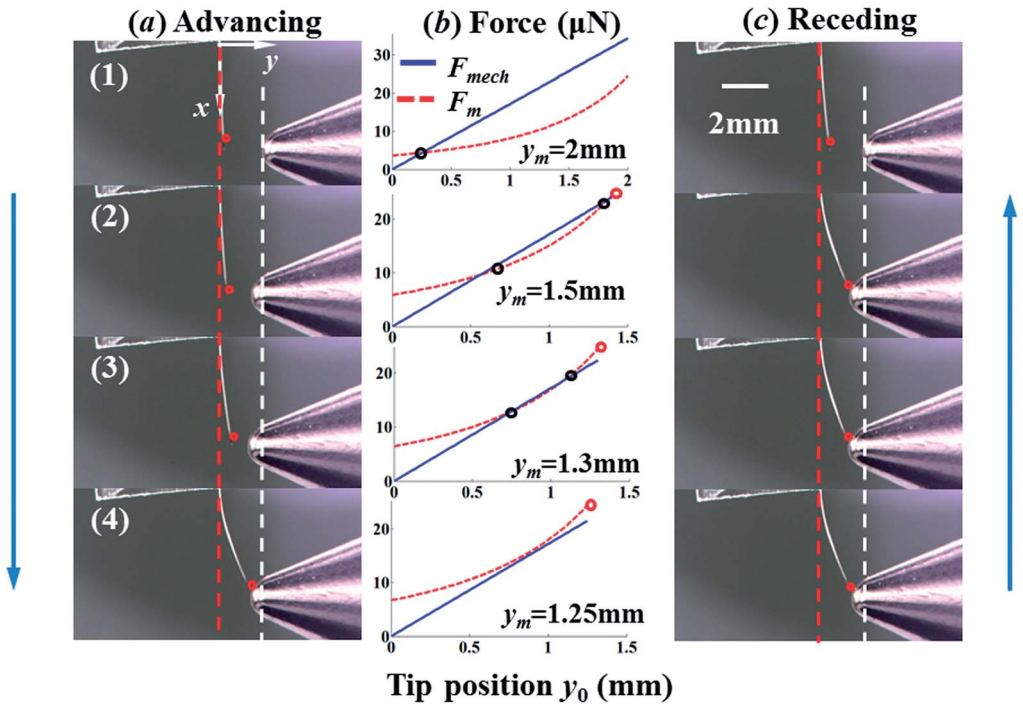

Fig. 5 Bending hysteresis of a 50 μm diameter Nylon fiber (POKEE) (a) magnet is advancing (b) the force diagram where the distance between the fiber tip and magnet, y_m, and position of the fiber tip, y_0 with respect to the clamped end were taken from experiments. (c) Magnet is receding.

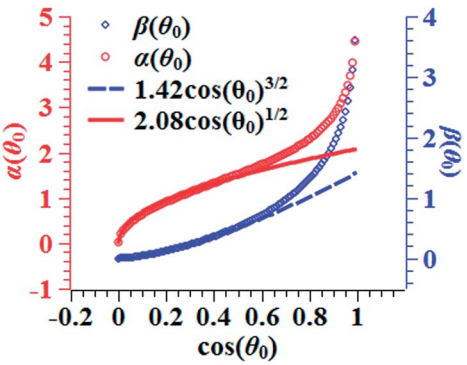

Fig. 6 Dependencies of $\alpha(\theta_0)$ and $\beta(\theta_0)$ and their approximations for small cos θ_0.

the fiber bow, we were able to estimate the elastic moduli of polymeric fibers at very low applied forces. Each fiber was tested 5 times and the average values were reported. Elastic modulus of all tested fibers show that the tensile test (Instron 1125) provides a greater elastic modulus relative to that obtained from the bending test with the magnetic force. This tendency is explained by the effect of orientation of polymeric chains at the greater Instron loads leading to the reinforcement of the fiber.[16] Table 1 summarizes the experimental data. Polymer chains in fibers are prone to align under tension: the larger the strain, the better the alignment.[17] The chain alignment leads to the fiber stiffening, *i.e.* to an increase of the fiber tensile modulus.[16] This effect of fiber stiffening is widely used in the cold drawing operation when the as-spun-fiber is subject to a tensile load. In the experiments conducted on Instron 1125, the instrument was able to provide the minimum tensile force of about 0.01 N. On the other hand, the maximum force applied in the bending experiment was about two orders of magnitude smaller, $\sim 10^{-4}$ N. Accordingly, the tensile tests are expected to cause much better chain alignment than the bending experiments do. Hence the modulus measured from the tensile test appears to be greater.

Table 1 Properties of three different fibers

Property	Nylon 66	Kevlar	Nylon (fishing line)
Young's modulus from the tensile test (GPa)	2.4	80.0	3.4
Young's modulus from bending experiments (GPa)	1.7	66.6	2.8
Diameter d (μm)	29	12.2	50
Flexural rigidity EI ($\times 10^{-10}$ Nm^2)	0.590	0.724	8.59
Fiber length L (mm)	0.98	2.51	5.09
Maximum applied force F_{max} (μN)	85	15	25
Dimensionless force $\gamma = F_{max}L^2/EI$	1.38	1.30	0.75

Materials and methods

Making the fiber tip magnetic

A ferrofluid (FerroTec) was mixed with 4 wt% polyethylene oxide (PEO) solution (Sigma-Aldrich, 1 000 000 Da) in a 1 : 1 weight ratio. This mixture provided a sufficiently high viscosity so that the droplet did not fall from the fiber tip. The main challenge in the deposition of small droplets on the fibers is that the adhesion forces are so high that the droplet is difficult to remove from the delivering fiber if the latter has a large diameter. We used a 75 μm Fluorocarbon fiber (Seaguar ACE) to deliver the droplet to the fiber with comparable diameters such as the Nylon fishing line and the glass fiber. For the fibers with very small diameters, we used the same type of fibers for the drop delivery. Since the wetting force is proportional to the fiber diameter, the thinner the fiber, the easier it is to remove the droplet from it.

In order to form a droplet, the fiber was dragged through the ferroglue mixture and a thin film was deposited on its surface. The film then collapsed into a series of droplets due to the Plateau–Raleigh instability.[18] Then the fiber of interest was brought in contact with the fiber containing the magnetic coating. The fiber to be tested was placed perpendicularly to the fiber with the magnetic coating. Moving the coated fiber to the left as shown in Fig. 7(a) and (b), one can form a big droplet at the end of the fiber to be tested. We waited at least 30 minutes until the droplet was completely dried guaranteeing that no magnetic material would be deposited on the magnet in the bending experiments. Fig. 7(c) and (d) confirm that the solid droplet preserved its shape after the bending experiment. Using ImageJ software (NIH), we confirmed that the volume of the droplet calculated from these two images was the same.

It should be noted that, the observed phenomena is not specific for the chosen experimental conditions but has a solid physical ground and can be reproduced with different magnets, beams, and magnetic tips. The type of a ferrofluid is not very important. The amount of the ferrofluid is much more important because the magnetic force at the fiber tip F_0 is proportional to the volume of the ferrofluid. One has to ensure that the relationship $F_0 L^3 \alpha\beta_m > 3EI$ is satisfied, otherwise the attachment/detachment hysteresis cannot be observed.

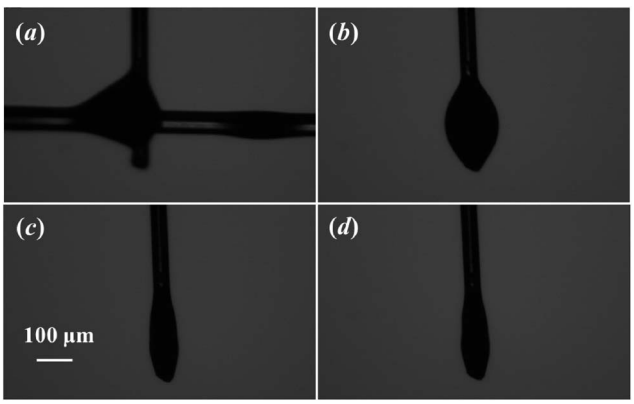

Fig. 7 (a) Collection of droplets on the fishing line (vertical) by moving the fluorocarbon fiber (horizontal) to the left. (b) Collected droplet sitting at the tip of the fishing line. (c) Magnetic droplet after drying for 30 minutes; (d) the same droplet after the bending experiment.

Magnetic characterization of the deposited droplets

Magnetic moments of the dried droplets were accurately measured by using the Alternating Gradient Magnetometer (AGM 2900, Princeton Measurements Inc., NJ, USA). Fig. 8 provides the confirmation that the droplets were superparamagnetic: the magnetization/field curve follows the Langevin dependence:[14]

$$m = m_0\left[\coth(\kappa B) - \frac{1}{\kappa B}\right], \quad m_0 = N\mu, \kappa = \frac{\mu}{k_B T}, \qquad (17)$$

where m is the magnetic moment of the droplet and B is the magnitude of the external magnetic field, N is the number of magnetic nanoparticles in the droplet, μ is the magnetic moment of a single nanoparticle, k_B is the Boltzmann constant, and T is the temperature.[14] For the same ferrofluid, parameter κ does not change. The pre-factor m_0 is proportional to the volume of the deposited droplet. We measured the magnetization curve for several ferrofluid droplets with different sizes.

It appeared that the Langevin function fits well the experimental data with the same $\kappa = 40T^{-1}$ and different parameters m_0 (Fig. 8(b)). The volumes of droplets estimated from Fig. 7(a) were $V = 2.51$ nL, 0.64 nL, and 1.41 nL respectively. Normalizing parameter m_0 by volume V, the magnetization pre-factor $M_p = m_0/V$ was obtained as $M_p = 45 \pm 4$ kA m^{-1}. By knowing the volume of the deposited droplet, one can obtain pre-factor m_0 and construct the magnetization curve using the Langevin function. Separation of these κ and M_p parameters makes the characterization of micro and nanofibers much easier: one does not need to measure the magnetization of very small droplets when magnetization is undetectable by the available magnetometers. Using the known κ-parameter and the m_0/V ratio, one needs to measure only the droplet volume. This is a much easier task and we have used optical microscopy for measuring the volume of microdroplets.

The conducted analysis allows one to significantly simplify the model needed for interpretation of the experimental data. In particular, the Langevin dependence suggests that the matrix of the dried droplet does not impose any anisotropy field and magnetic moments of individual nanoparticles exactly follow the applied magnetic field. In other words, the magnetic moment of the deposited droplet should be co-aligned with the applied field. Hence only the bending force was exerted on the fiber, and one would not have any spontaneous torque associated with the misalignment of the magnetic moment with the field.[19,20]

Distribution of the magnetic field

The distribution of magnetic field generated by the magnet was difficult to measure with the available teslameters because the tip of the magnet was much smaller than the probe size. We therefore calculated the distribution of magnetic field in the vicinity of the magnet pole using COMSOL® 4.2. In all calculations, a uniform magnetization M_s of the magnet in the

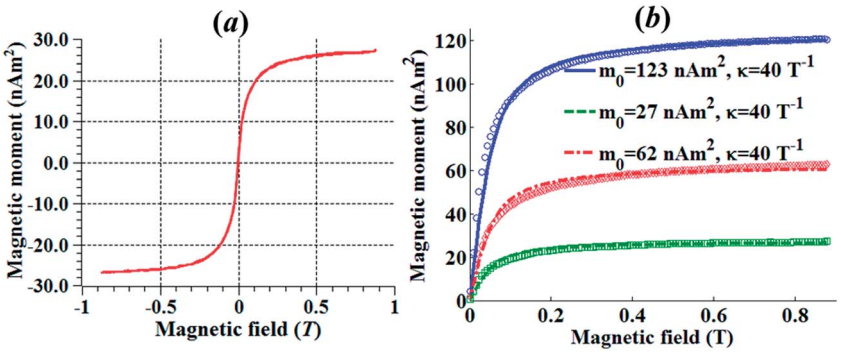

Fig. 8 (a) An example of the magnetization/field curve taken by AGM on a dried magnetic droplet (b) the experimental data points approximated by the Langevin function for three different magnetic droplets with different volumes *V*.

y-direction was assumed. Considering magnetization M_s as an adjustable parameter, one can generate the field distributions and calculate the magnetic force for each M_s using eqn (1). Fig. 3 shows an example of distribution of the magnetic field around a hemispherical magnetic pole attached to a conical magnet. In this numerical experiment, we used magnetization $M_s = 1.1 \times 10^6$ A m^{-1}. Thus, the distribution of magnetic field around the magnet can be completely described by specifying a single characteristic of the magnet, its magnetization M_s.

Bending of the elastic fiber by the magnetic field

For the calibration of the experimental setup and for the specification of the magnetization M_s, we used a 100 μm diameter glass fiber (Corning). The Young's modulus of the glass fiber was determined by applying a known weight W to the fiber end ($F_{mech} = W$). The elastic modulus was obtained as $E = 17.0$ GPa. From the Euler elastica equation and boundary conditions, the ratio F_{mech}/EI completely describes the shape of the deformed fiber.[15] Therefore, fitting the profile of the fiber bow with the numerical solution of eqn (10), one can extract the ratio F_{mech}/EI.

The magnetic moment of the deposited droplet was measured independently as discussed above. The magnet was moved along the *y*-axis and stopped at several positions so that a series of equilibrium configurations of the fiber can be obtained, Fig. 4. Using this series of pictures with different equilibrium configurations of the glass fiber, we fitted the fiber profiles with the Euler elastica model considering magnetization M_s of the magnet as an adjustable parameter. Ten different equilibrium configurations of the fiber were used for calibration and the magnetization was determined as $M_s = (1.1 \pm 0.2) \times 10^6$ A m^{-1}.

In the paper, we used a single fiber to illustrate the idea of a magnetic grabber. However, fiber bundles, yarns, and fibrous strips are able to flex in a similar way and their bending behaviour can also be described by the Euler elastica equation.[5–7,10–12] Hence, one expects to observe the similar attachment/detachment hysteresis on these grabbers. To make the tip magnetic one can simply dip a yarn or a fibrous strip into a magnetic glue as demonstrated in ref. 5. A single magnetic droplet can be formed at the tip of a yarn or a fibrous strip.[5] Hence the same theory is applicable for more complex fibrous grabbers with a magnetic tip.

Conclusion

We developed an experimental protocol to study the behavior of a magnetic grabber formed by a fiber with a magnetic droplet deposited on the fiber tip. When a permanent magnet moves toward the fiber it creates micro or even nano-Newton level forces. It has been shown that these forces are sufficient to drag the fiber to the magnet. The fiber tip follows different pathways when the magnet approaches and when it retracts from the fiber. This phenomenon was successfully explained by the Euler–Bernoulli model of the elastic beam. The observed hysteresis of fiber attachment to/detachment from the magnet was attributed to the multiple equilibrium configurations of the fiber tip placed in a dipole-type magnetic field. Four different fibers were tested and the attachment/detachment hysteresis was proved to be a universal property of the fiber-based magnetic grabber controlled by a magnet generating a dipole-type field configuration. This protocol can be used for characterization of mechanical properties of microfibers and nanofiber bundles at very low loads when available methods fall short.

Acknowledgements

This work was supported by the US Air Force Office of Scientific Research, Grant FA9550-12-1-0459 and by the US National Science Foundation, Grant PoLS 1305338.

Notes and references

1 K. K. Chawla, *Fibrous materials*, Cambridge University Press, Cambridge, England, New York, 1998.
2 T. Hongu, G. O. Phillips and M. Takigami, *New millenium fibers*, Woodhead Publishing Ltd, Cambridge, England, 2005.
3 D. B. Newell, J. A. Kramar, J. R. Pratt, D. T. Smith and E. R. Williams, *IEEE Trans. Instrum. Meas.*, 2003, **52**, 508–511.
4 L. Stenlund, K. Riski, J. Seppa, M. Pudas, M. Vahasoyrinki, V. Tuhkanen and J. Roning, *Meas. Sci. Technol.*, 2010, **21**, 075102.

5 C.-C. Tsai, P. Mikes, T. Andrukh, E. White, D. Monaenkova, O. Burtovyy, R. Burtovyy, B. Rubin, D. Lukas, I. Luzinov, J. Owens and K. Kornev, *Nanoscale*, 2011, **3**, 4685–4695.
6 R. E. Groff, H. Karve, M. Li, A. Tokarev and K. G. Kornev, *J. Eng. Fibers Fabr.*, 2012, **7**, 74–83.
7 A. Cebers, *Curr. Opin. Colloid Interface Sci.*, 2005, **10**, 167–175.
8 R. Dreyfus, J. Baudry, M. L. Roper, M. Fermigier, H. A. Stone and J. Bibette, *Nature*, 2005, **437**, 862–865.
9 O. S. Pak, W. Gao, J. Wang and E. Lauga, *Soft Matter*, 2011, **7**, 8169–8181.
10 F. C. Moon and Y. H. Pao, *J. Appl. Mech.*, 1969, **36**, 92–100.
11 F. C. Moon and Y. H. Pao, *J. Appl. Mech.*, 1968, **35**, 53–58.
12 F. C. Moon and P. J. Holmes, *J. Sound Vib.*, 1979, **65**, 275–296.
13 K. Singh, C. R. Tipton, E. Han and T. Mullin, *Proc. R. Soc. A*, 2013, 469.
14 R. E. Rosensweig, *Ferrohydrodynamics*, Cambrige University Press, Cambrige, 1985.
15 L. D. Landau, E. M. Lifshitz, A. d. M. Kosevich and L. P. Pitaevskii, *Theory of elasticity*, 3rd English edn, Pergamon Press, Oxford Oxfordshire, New York, 1986.
16 *Structure Formation in Polymeric Fibers*, ed. D. R. Salem, Hanser Gardner, Cincinnati, 2001.
17 I. M. Ward and J. Sweeney, *An introduction to the mechanical properties of solid polymers*, Wiley, Chichester, West Sussex, England, 2nd edn, 2004.
18 P. G. Drazin and W. H. Reid, *Hydrodynamic stability*, Cambridge University Press, Cambridge, UK, New York, 2nd edn, 2004.
19 J. J. Newman and R. B. Yarbroug, *J. Appl. Phys.*, 1968, **39**, 5566–5569.
20 E. Blums, A. Cebers and M. M. Maiorov, *Magnetic fluids*, Walter de Gruyter, New York, 1997.